

FIRBACK II. Data Reduction and Calibration of the 170 μm ISO* Deep Cosmological Survey

Guilaine Lagache¹ and Hervé Dole^{2,1}

¹ Institut d'Astrophysique Spatiale, Bât. 121, Université Paris XI, 91405 Orsay Cedex, France

² Steward Observatory, University of Arizona, 933 N Cherry Ave, Tucson, AZ, 85721, USA

Received 24 January 2001; Accepted 5 March 2001

Abstract. We present the final reduction and calibration of the FIRBACK ISOPHOT data. FIRBACK is a deep cosmological survey performed at 170 μm . This paper deals with the ISOPHOT C200 camera with the C160 filter. We review the whole data reduction process and compare our final calibration with DIRBE (for the extended emission) and IRAS (for point sources). The FIRBACK source extraction and galaxy counts is discussed in a companion paper (Dole et al. 2001).

1. Introduction

With more than 150 hours of observations, FIRBACK (Far-InfraRed BACKground) is one of the largest observational programmes made with the ISOPHOT instrument on board the Infrared Space Observatory (ISO) satellite. This cosmological deep survey at 170 μm covers more than 4 square degrees located in two Northern and one Southern fields (Lagache 1998, Dole 2000a). There are 106 sources detected above the sensitivity limit (180 mJy, 4σ). The number of sources detected above 135 mJy (3σ) is 196. The first result of this survey is the high number of sources observed when compared to no, or moderate, evolution models for infrared galaxies (e.g. Dole 2000a). Preliminary results in the so-called Marano1 field were published in Puget et al. (1999), and on the whole survey by Dole et al. (2000b). FIRBACK also allows for the first time the detection of the CFIRB fluctuations (Lagache & Puget 2000; Puget & Lagache, 2001).

After a presentation of the observational issues of the FIRBACK survey, we present in this paper the final stage of the data reduction and calibration. We use the Phot Interactive Analysis (PIA, Gabriel et al. 1997) for the standard reduction and calibration (Sect. 3.1) with some extra developments: flat-fielding, transient corrections and reprojection (Sect. 3.2-3.7). In Sect. 4, we review our final map calibration and compare it with absolute photomet-

Table 1. FIRBACK fields main characteristics

Field	l deg	b deg	surface deg ²	t_{int} sec	Number of rasters
FSM	270	-52	0.95	256	2×11
FN1	84	+45	1.98	128	2×9
FN2	65	+42	0.96	128	4×4

ric calibration from other instruments. We then conclude in Sect. 5.

2. FIRBACK observations

FIRBACK covers about 4 square degrees in 3 high galactic latitude fields (chosen to have very low HI column density, typically $N_{HI} \leq 10^{20} \text{cm}^{-2}$), the so-called N1 (FN1), N2 (FN2) and Marano (FSM) fields. The observations were performed at an effective wavelength of 170 μm with the C200 array (2x2 pixels) of ISOPHOT. The pixel field of view is 1.5 arcmin. We use the AOT (Astronomical Observation Template) PHT22 in the multi-pointing staring raster mode. Each FIRBACK field (Table 1) consists of several rasters of 17×17 pixels¹:

- Eleven rasters were done in the so-called FN1 field. These rasters were re-observed with a shift in position that corresponds to a fraction of an ISOPHOT pixel to provide proper sampling where possible. Observations were done from the ISO revolution 753 to 774. This field covers the same area as the ELAIS N1 15 μm and 90 μm observations (Oliver et al. 2000).

Send offprint requests to: Guilaine.Lagache@ias.u-psud.fr

* Based on observations with ISO, an ESA project with instruments funded by ESA Member States (especially the PI countries: France, Germany, the Netherlands and the United Kingdom) and with the participation of ISAS and NASA.

¹ Except for the FSM1 field (Puget et al. 1999) where the rasters are 19×19 pixels

- Nine rasters were done in the so-called FN2 field. These rasters were again re-observed with a shift in position. The field covers the same area as the ELAIS N2 15 μm and 90 μm observations. These data are FIRBACK/ELAIS observations. They were done from the ISO revolution 785 to 798.
- One raster was observed in the so-called FSM1 field (formerly called Marano 1 field) during the revolution 593 and three rasters in the so-called FSM234 field (from revolution 739 to 744). Rasters have been observed four times. Displacements between the four independent observations correspond to about 0.5 pixel, except for the FSM1 field where the displacements correspond to 2 pixels (note that the overlapped surface with the “original” Marano field is less than 15%).

Each raster is performed in the spacecraft (Y, Z) coordinate system which is parallel to the edges of the detector array, with one pixel overlap in both Y and Z direction. The exposure time is 16s per pixel and thus 128, 128 and 256s per sky position in the FN1, FN2 and in the FSM fields respectively.

We also have a PHT25 measurement in the FSM1 field. This AOT is the absolute photometry mode for PHT-C, in which photometric calibration is achieved by chopping against the internal fine calibration source. For low fluxes (i.e. in our case), chopping is also done against the switched-off “Fine Calibration Source”, which has a temperature level of about 4K. This is the temperature of the optical support on which the instrument is mounted. Such a measurement serves to define a zero point. This mode is especially well suited for observations aiming at accurate determination of the absolute brightness of the background emission.

3. Data reduction

3.1. PIA data reduction and calibration

We use PIA, the ISOPHOT Interactive Analysis software version 7.2.2 (Gabriel et al. 1997), to correct for instrumental effects, the glitches induced by cosmic particles and to provide an initial calibration. First we apply the non-linearity correction due to 2 independent effects: the non-linearity of the Cold Readout Electronics and the downward curving ramp due to de-biasing. Deglitching is performed for each individual ramp and then the mean signal per position is derived by averaging the ramp slopes (we do not apply any transient correction at this stage). We then apply a second deglitching (for every chopper position, a “running mean” method is applied; signals that are far away by a number of sigma, typically 5, are flagged). The dark current, which represents less than 5% of the signal, is subtracted using the orbit dependent calibration files. We also apply the “reset interval correction”, a correction which represents less than 6% of the signal.

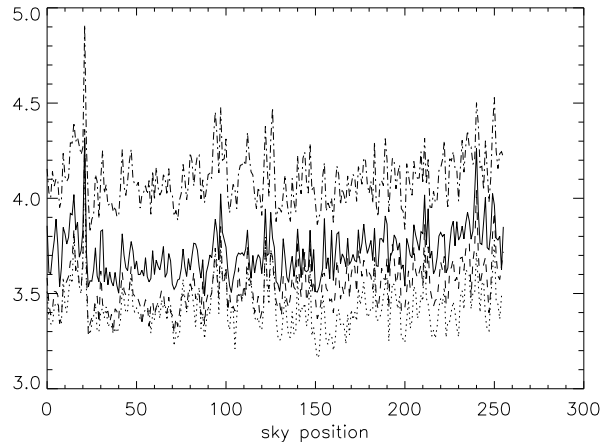


Fig. 1. Signal in MJy/sr of the four pixels as a function of the sky position for one raster. The mean signal level is not the same (no flat-field correction has been applied at this stage) but the signal variations are highly reproducible.

We do exactly the same data reduction for the two “Fine Calibration Source” (FCS) measurements. The FCS measurements before and after the observation vary by less than 3% for most of the rasters. We decide to perform the first calibration (from V/s to MJy/sr) by deriving the mean value of the two FCS measurements. We prefer not to use the interpolation between the two FCSs when they are different since it may induce Long Term Transients (LTT) that are not necessary real. On the contrary, when real, the interpolation between the two FCSs could correct for the LTT, but we prefer to correct the LTT following Sect.3.3.

At this stage of the data reduction, we have the signal variation (in MJy/sr) as a function of time (or position) for each pixel in each raster. We see from Fig. 1 that the instrumental noise is very low. We have, per sky position, a very high reproductibility of the data.

3.2. The PHT25 measurement

The AOT PHT25 absolute measurement in the FSM1 field has the following characteristics (Fig. 2):

- 256s for the “sky dark”: observation of the cold opaque filter
- 128s for the “FCS dark”: observation of the cold FCS (turned off)
- 256s on sky
- 256s on the FCS

With this measurement we check that:

- The FCS value after 256s and the one obtained with 32s integration time (which is the integration time in the PHT22 observations) differs by less than 4%
- The difference between the observed dark current (“sky dark”) and the default PIA one is less than 10%

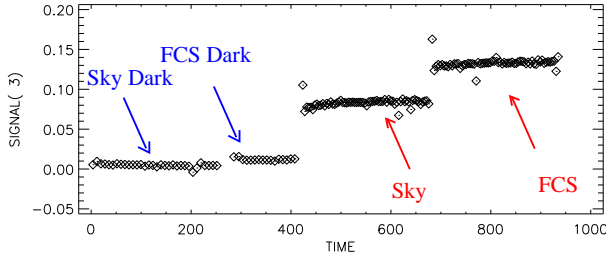


Fig. 2. Absolute PHT25 measurement sequence for one pixel (in V/s)

- The difference between the FCS dark current (“FCS dark”) and the default PIA one is less than 2%

We obtain for the sky measurement a brightness² of 3.10 ± 0.14 MJy/sr, to be compared to the value measured on the final map (Fig. 6), which is 3.08 MJy/sr. We have a very good agreement between both measurements; we do not observe any significant discrepancy between the “raster mode” observations and the “absolute mode” one.

3.3. Long term transients

Long Term Transients (LTT) still have an unknown origin. They are observed on a characteristic time scale of about 60-80 minutes and are the main sensitivity limitation of the ISOCAM diffuse emission analysis (Miville-Deschênes et al. 2000). LTT are observed in FIRBACK data (Fig. 3) but only for some rasters and pixels. We first tried to correct the LTT using the method developed by Miville-Deschêne et al. (2000) for ISOCAM; however, this method fails since (1) ISOCAM and ISOPHOT detectors are different and (2) the redundancy in our observations is too low. The method developed for ISOCAM clearly detects the long term variation. However, for ISOPHOT, all detectors are not contaminated by the LTT (we see Fig. 3 that the LTT is not seen by the four pixels), which is not the case for ISOCAM, where all detectors have at a first order the same behaviour. Therefore, we correct the LTT by assuming that the pixel, in each raster, that exhibits the smallest long term variation (or smallest slope) is representative of the sky. Fig. 3 shows the results before and after the correction.

3.4. Individual raster flat-fielding

The flat-field correction, for each individual raster, is directly estimated using the redundancy of our observations and comparing position by position the brightness of the 4 pixels. First, for each raster, we compute the responsivity of the four pixels with respect to the mean responsivity (Fig. 4) for each sky position. We see from Fig. 4 that each pixel has some high frequency instrumental noise. What

² We correct the brightness for the flat-field using the average values given in Sect. 3.4 and apply the extended calibration factor correction (Sect 4.3).

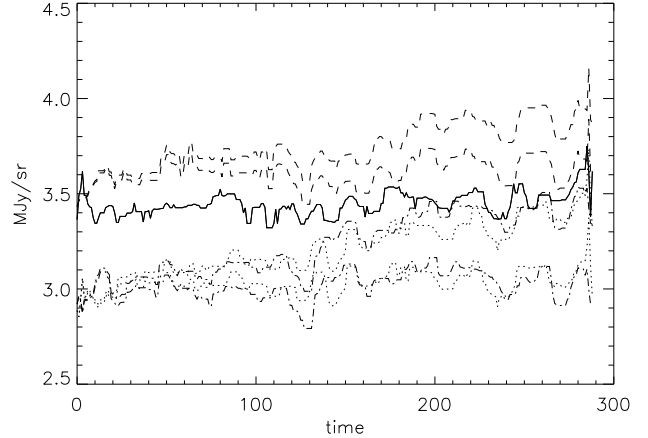


Fig. 3. Illustration of the LTT correction on a 17×17 raster. The thick solid line is the pixel signal (median filtered over 9 position) with the smallest slope. The long term variation of the three other pixel signals (thin lines: dot, dot-dash, dash) are corrected in order to follow the same slope as the continuous line pixel signal. The result after correcting the slope is shown in thick lines. Note here that the signal of each pixel is not offsetted after the LTT correction (this is the flat-field correction detailed in Sect. 3.4).

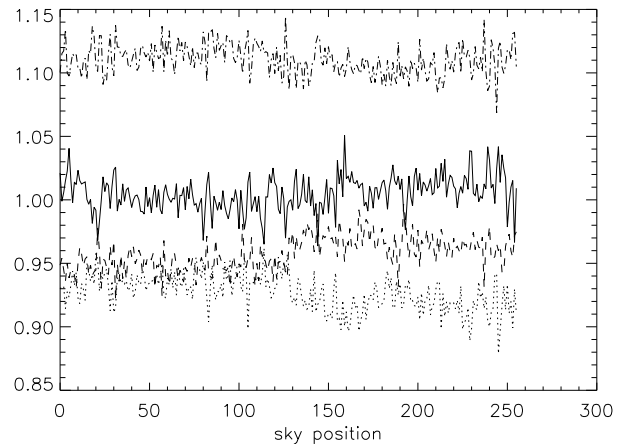


Fig. 4. Relative response of the 4 pixels as a function of the sky position. The flat-field correction is obtained by computing a 30-points running median (and the mean correction is equal to 1).

we are interested in is the low-frequency difference of responsivity between the four pixels. Therefore, we derive the flat-field correction by computing a 30-points running median (and the mean of the correction is equal to 1 per sky position).

The correction is rather constant for the whole 56 rasters and equal on average to: 1.04 ± 0.02 , 0.91 ± 0.02 , 1.09 ± 0.02 and 0.94 ± 0.02 for pixel 1, 2, 3 and 4 respectively. This highly reproducible behaviour may be used to correct for the flat-fielding in any other C-160 observation that has no redundancy.

3.5. Transients induced by energetic cosmic rays

The procedure described in Sect. 3.4 also reveals some long term transients induced by energetic cosmic rays, as can be seen in Fig. 4 for the dashed line signal around the sky position number 130. These effects induced by energetic cosmic rays are quite rare: we detect only 13 events for FIRBACK (to be compared to 4 detectors \times 56 rasters = 224 timelines). After such a cosmic ray, the signal may show an exponential-like behaviour (with a variable time constant). We correct for such events manually before computing the flat-field correction.

3.6. Short term transients

After a sudden increase of flux, most infrared detector signals shows an instantaneous jump followed by a slow rise to the stabilisation level; this is the short term transient. In most observations, the stabilisation level is never reached, due to the limited integration time per chopper plateau.

For the ISOPHOT C200 camera, we have information on the short term transients using our PHT25 absolute measurements. We see in Fig. 5 the signal behaviour of the PHT25 sky measurements for the 4 pixels. These measurements follow the “FCS dark” observation, whose signal is 10 times weaker (see Fig. 2). We clearly see in Fig. 5 a short term transient before the stabilisation. The instantaneous signal jump is of the order of 85%; and the stabilisation is reached in several tens of seconds.

For FIRBACK field observations, the short term transient effect is limited due to the flatness of the fields. Flux variations are very smooth and weak, except when point sources are observed. Therefore, no correction is applied for the diffuse emission. In return, for point sources, a correction of 10% is applied (this 10% is derived using the flux measured after 16s FIRBACK integration time compared to the stabilised flux).

For the FCS FIRBACK measurements, no correction is applied since (1) the difference between the stabilised signal in the PHT25 FCS measurement and the one measured in 32s (which is the integration time on the FCS) is less than 4 % and (2) the second FCS observation is at the same level as the FIRBACK sky observation (no flux step) and the two FCS measurements (before and after one observation) differ by less than 3% for most of the rasters.

3.7. General “flat-fielding”

The different rasters in the same field have been done at different time (there can be several months between the rasters). Therefore, the absolute calibration performed using the FCS measurements can be slightly different from one raster to another. This difference is observed in the final FIRBACK maps as discontinuities between

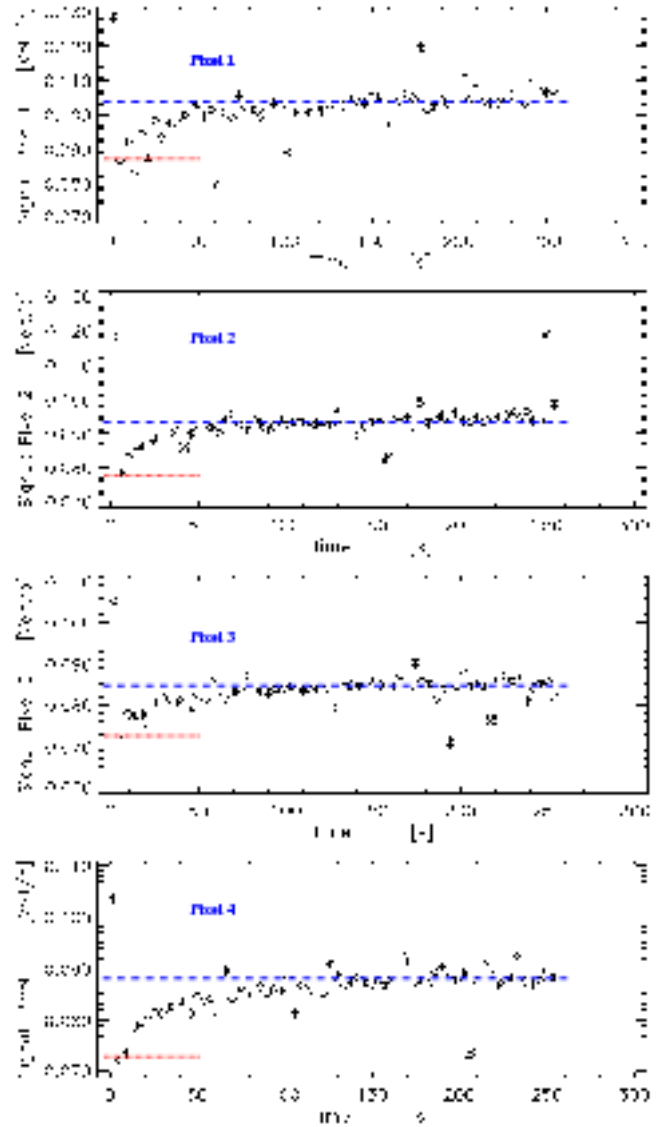


Fig. 5. Signal variation after a flux step (PHT25 sky measurements that follow the “FCS dark” measurements). For all pixels, the instantaneous jump is at the \sim 85% level and the stabilisation is reached in about 80s.

individual rasters.

To correct for this small absolute calibration difference, we apply a “general flat-field” correction in order to make consistent the level of each raster with its neighbourhood. This correction consists of adding or subtracting offsets, the sum of the offsets being 0. This effect is very small, less than 5%, except for one raster in FN1 which shows a discontinuity with its neighbourhood of about 11%.

3.8. Reprojection

The flux is finally projected on a $10'' \times 10''$ coordinate grid using our own projection procedure. The procedure is the following:

- We compute each individual pixel coordinates.

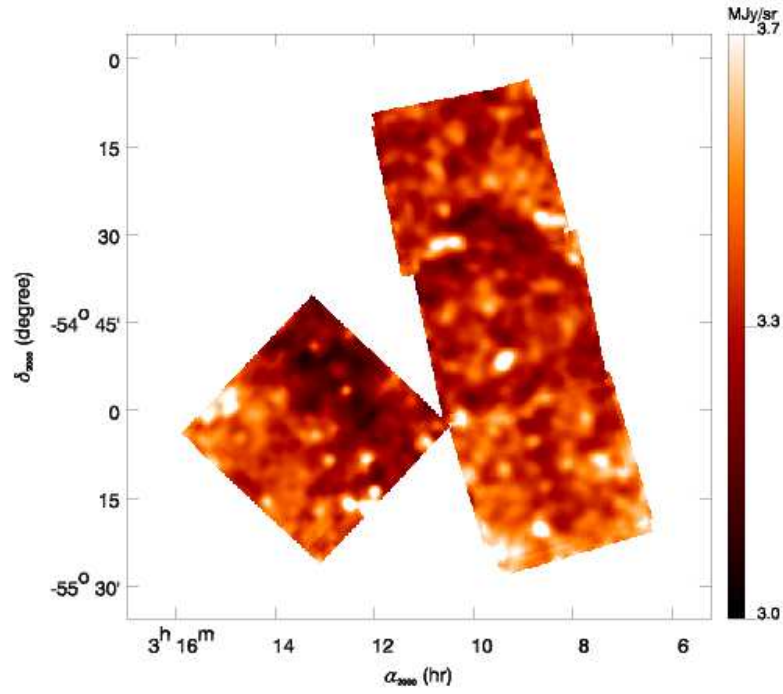


Fig. 6. Map of the FIRBACK South Marano (FSM) field. FSM1 is the square on the left, and the rectangle is composed of FSM2, 3 and 4 from top to bottom.

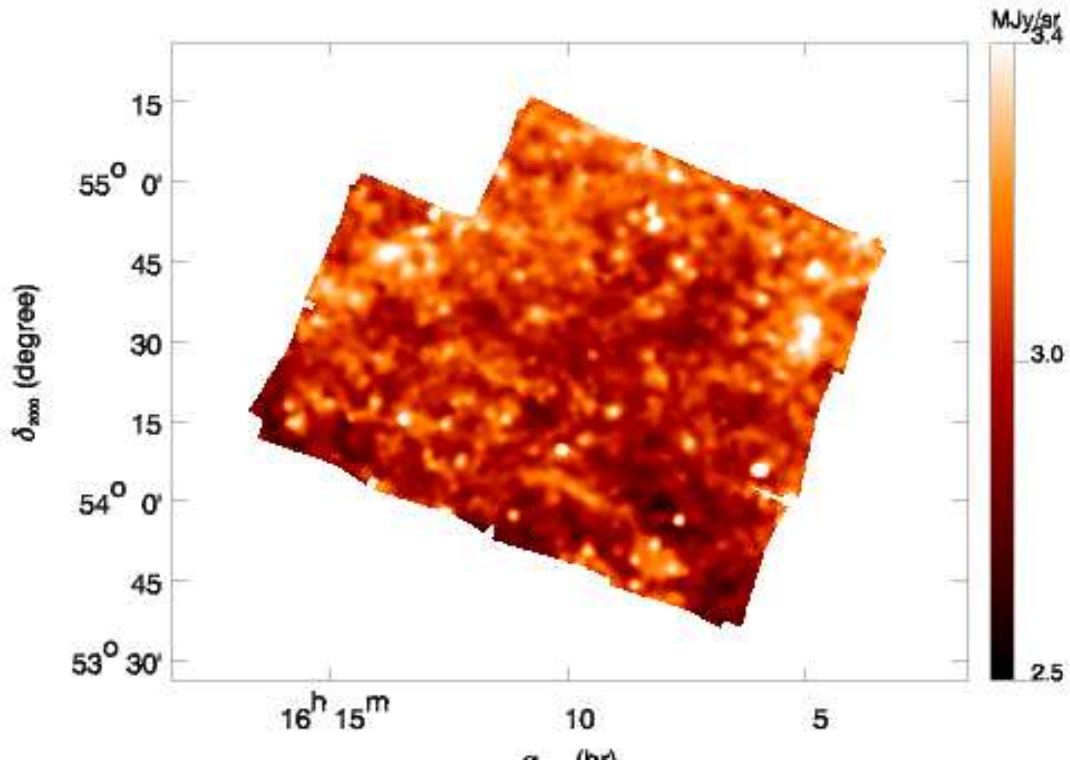


Fig. 7. Map of the FIRBACK North 1 (FN1) field.

- We create individual maps for each pixel and raster with 2D $\frac{\text{sin}x}{x}$ interpolation for the oversampling signal and bilinear interpolation for the coordinates.
- We compute for each field the final coordinate grid (10" sampling) using the individual raster coordinates

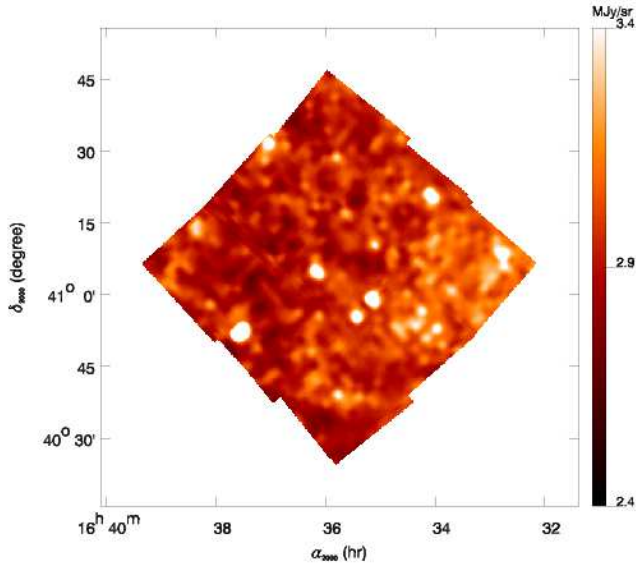


Fig. 8. Map of the FIRBACK/ELAIS North 2 (FN2) field.

- At each final grid point, we add the observed signal and compute the weight and variance.

We have checked the accuracy of our method using simulated sky maps, containing both extended emission and point sources. Our reprojection does not change the background brightness and the sources flux (at the 1% level). One has, however, to note that this method is particularly well adapted to cosmological observations: weak sources on a rather flat background (for fields with very bright sources, this method may not preserve the point source photometry).

The final maps are shown in Fig. 6, 7 and 8 for the three fields respectively.

4. Calibration

The extended emission calibration has changed by a factor of about 2 between PIA version 6 and PIA version 7. A large part of this factor comes from the different footprint solid angle values used in the different PIA versions.

4.1. Footprint observations around Saturn

During the revolution 409, ISOPHOT made several tens of pointing around Saturn at distances between 4.2 and 45.4 arcmin in order to map the extended wings of the PHOT footprint at $170 \mu\text{m}$ during about 5 hours. Observations were made in the Y and Z satellite axis directions. Fig 9 shows the observed pattern on an IRAS $100 \mu\text{m}$ map. All directions were observed twice, back and forth. Observations were performed with the following AOTs: PHT 37-38-39 (sparse maps; PHT37: FCS; PHT38: sky; PHT39: FCS) for distances between 4.2 and 27.6 arcmin, and PHT25 (absolute photometry) at the largest

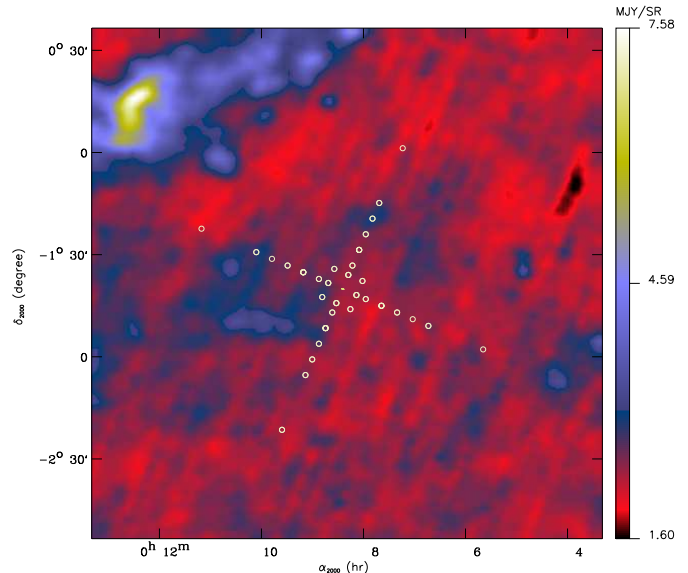


Fig. 9. ISOPHOT pointing positions (circle) around Saturn on the IRAS $100 \mu\text{m}$ map. Saturn positionnal changes during the observations have been computed using the ephemerids of the Bureau des Longitudes (Berthier, 1998) and are represented by a small segment at the middle of the cross.

distance. Integration times are around 150 sec for PHT38, 200 sec for PHT37-39 and 400 sec for PHT25.

We use PIA V7.2.2 for the data reduction and calibration. For each detector and each position, we keep only the second half of the data corresponding to the stabilised signal. These observations have no transients induced by cosmic rays and we do not apply any flat-field correction. Sixty seven files were used, the others being either unreadable (3 files) or saturated (3 files). Results are presented in Fig. 10 and 11 for all data in the Y and Z direction respectively. Each pixel is plotted and is used as an independent measurement.

4.2. Comparison of the footprint model with Saturn observations

A model for the ISOPHOT footprint has been developed at Heidelberg (Klaas et al., private communication) based on the ISOCAM footprint routines. This model includes the optical characteristics of the telescope, the primary and secondary mirrors, and the filters and detectors. We have used this program to compute the ISOPHOT footprint up to 20 arcmin with the $170 \mu\text{m}$ bandpass filter. Results of the model are shown in Fig. 12 together with the Saturn measurements for the Z axis. To make this comparison, we have assumed for Saturn a flux of 32000 Jy and removed the background using the PHT25 measurement.

We see a very good agreement between the model and the measurements. However, around 4.5 arcmin from Saturn, some data, coming from one Y direction scan (only one position), have a significantly higher flux than the

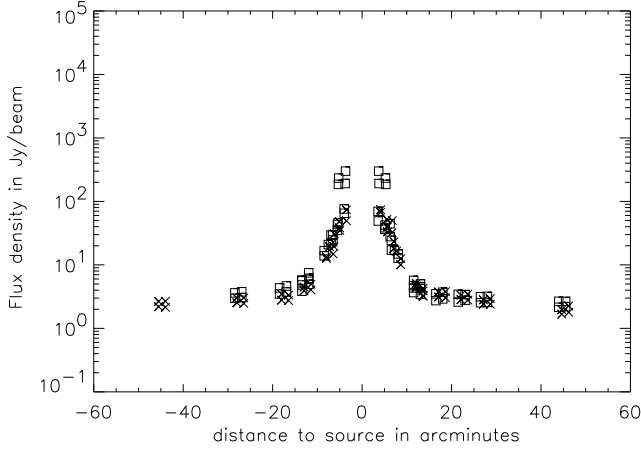


Fig. 10. Y direction measurements around Saturn. Squares are forward data, crosses, backward data. Dispersion between the 4 pixels at each position comes mainly from the non correction of the flat-field.

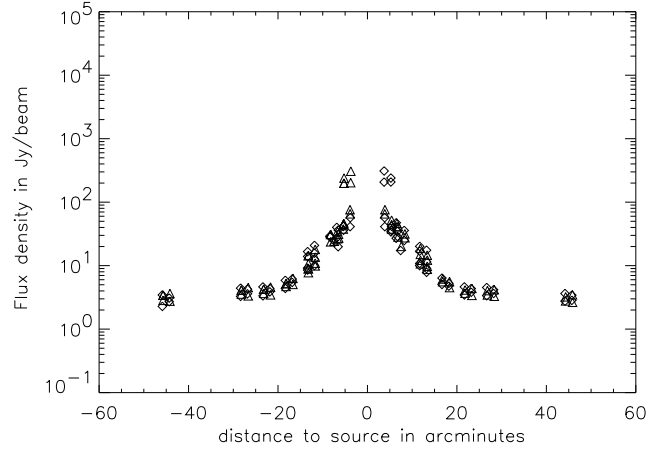


Fig. 11. Z direction measurements around Saturn. Triangles are forward data, diamonds, backward data.

model prediction. Data at similar distances from Saturn in other scans cannot be used due to saturation problems. Therefore, we interpret this discrepancy as due to detector saturation problems (one can note, however, that the contribution of these data points to the solid angle is lower than a few percent).

In conclusion, the ISOPHOT footprint measurements and model at $170 \mu\text{m}$ are in very good agreement. We therefore use, in the following, the model (from Klaas et al., private communication) as the definitive footprint at $170 \mu\text{m}$.

4.3. The extended brightness photometric correction factor

In PIA V6.5 the solid angle used to convert the flux in brightness was that of the pixel ($1.88 \cdot 10^{-7}$ sr); in PIA V7.2.2, it is the footprint model's one but truncated at 4.1 arcmin ($2.73 \cdot 10^{-7}$ sr). The full solid angle of the footprint is equal to $3.06 \cdot 10^{-7}$ sr. Therefore, there is a photometric correction factor to be applied to the extended emission:

$$B_\nu = B_\nu(\text{piaV72}) \times \frac{\Omega_{\text{piaV72}}}{\Omega_{\text{footprint}}}$$

$$B_\nu = B_\nu(\text{piaV72}) \times 0.89$$

After correction of the absolute calibration of the extended emission, point source fluxes (given in Dole et al. 2001) are computed using the footprint model (Klaas et al., private communication).

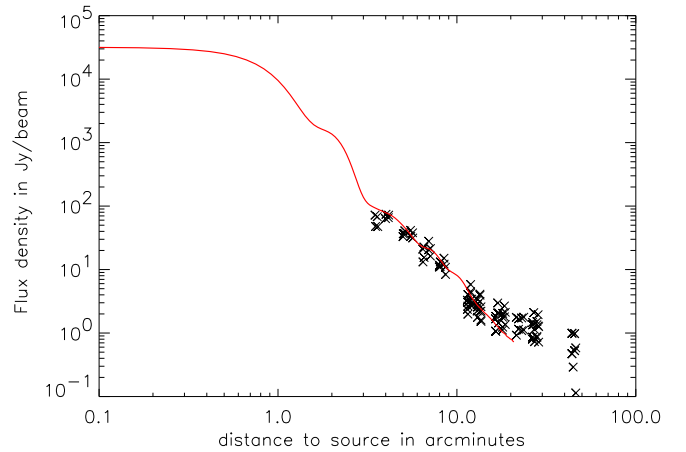


Fig. 12. ISOPHOT footprint model (continuous line) compared to ISOPHOT measurements around Saturn for the Z axis.

4.4. The rejection rate

Unique measurements have been done by the ISOPHOT team during the eclipse of the sun by the earth (Kranz et al. 1998; Klaas et al. 1998a; Lemke et al. 1998) by pointing at a sky region at 60° from the sun before, during, and after the eclipse. These measures reveal no signal variation, leading to an upper limit of 10^{-13} at 60° for the stray-light rejection rate. This exceptional measurement clearly shows that there is no contribution to the flux from the far-side lobes. This demonstrates that ISO is able to make

Table 2. Cosmic Infrared Background (CIB) from Lagache et al. (2000), zodiacal (from Reach et al. 1995) and dust emission (from Lagache et al. 2000) at $170\ \mu\text{m}$ for the three FIRBACK fields (in MJy/sr). The total emission is the sum of the three contributions for each field. There is a remarkable agreement between the predicted brightness and the measured ISOPHOT one.

	FN1	FN2	FSM
CIB	1.10 ± 0.2	1.10 ± 0.2	1.10 ± 0.2
Zodiacal	0.71 ± 0.1	0.80 ± 0.1	0.75 ± 0.1
N_{HI} (cm^{-2})	$8.2\ 10^{19}$	$7.7\ 10^{19}$	$1.0\ 10^{20}$
Dust	1.17 ± 0.35	1.09 ± 0.33	1.42 ± 0.43
Total predicted	2.98 ± 0.41	2.99 ± 0.40	3.27 ± 0.48
PHOT measured	3.01 ± 0.14	2.97 ± 0.17	3.39 ± 0.12

absolute measurements of the extended emission and gives a high degree of confidence to our absolute photometric calibration.

4.5. Comparison with DIRBE extended brightness

We can now compare the extended ISOPHOT FIRBACK brightness with the predicted one using DIRBE and HI measurements. Because of the size of the DIRBE beam, this comparison is only feasible due to the flatness of the FIRBACK fields; this flatness is observed with DIRBE on several degrees around each FIRBACK field.

The sky measurement is the sum of the zodiacal light, Cosmic Infrared Background (CIB) and dust interstellar emission. For each field the zodiacal light, at the time of the observation, has been computed using the Reach et al. (1995) DIRBE model. The CIB is extrapolated at $170\ \mu\text{m}$ using the DIRBE measurements of Lagache et al. (2000). For the dust emission, we compute its contribution using (1) the HI column density from the Leiden-Dwingeloo survey, Hartmann & Burton 1997 (we prefer to use the HI column density rather than the DIRBE brightness since DIRBE data are very noisy in FIRBACK fields) and (2) the emissivity from Lagache et al. (2000). The final predicted emission at $170\ \mu\text{m}$ for the three fields is shown in Table 2. It is in remarkable agreement with the measured ISOPHOT brightness³.

4.6. Comparison with IRAS point sources measurements

The absolute flux calibration of ISOPHOT is derived using calibration standards such as planets, asteroids or stars (Klaas et al. 1998b; Schulz et al. 1999; ISO Consortium 2000a, 2000b). One can however check, using IRAS detected sources in FIRBACK fields, the consistency between IRAS 60 and $100\ \mu\text{m}$ flux and the

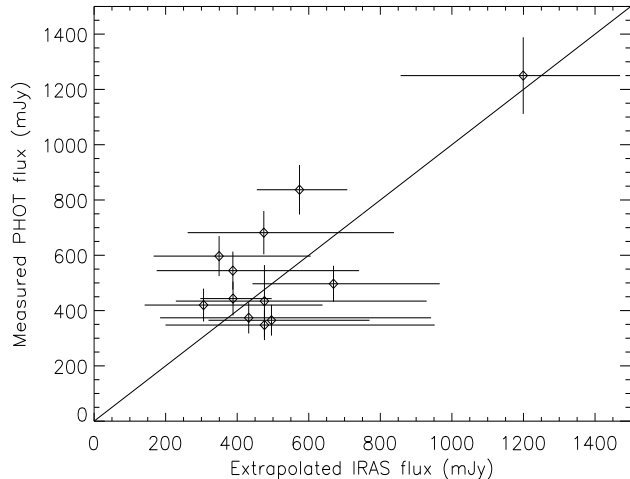


Fig. 13. Comparison of the ISOPHOT $170\ \mu\text{m}$ measured flux with the IRAS extrapolated ones. Data are compatible with a slope of unity.

ISOPHOT $170\ \mu\text{m}$ one. However, we have to keep in mind that it is very difficult to extrapolate the IRAS fluxes at $170\ \mu\text{m}$ (one can have a factor 2 to 3 in the extrapolation using different models or black-body temperatures).

Twelve FIRBACK sources, well identified as very nearby non interacting galaxies, have IRAS 60 and $100\ \mu\text{m}$ flux counterparts, measured with SCNAPI⁴. We extrapolate the 60 and $100\ \mu\text{m}$ IRAS flux using the template spectra of Dale et al. (2000). These spectra are based on the IRAS 60/100 color ratio and are thus well adapted. The comparison is shown on Fig. 13. Uncertainties on the extrapolation, that take into account only the errors on the 100 and $60\ \mu\text{m}$ fluxes (and not the model uncertainty), are very large. Data are compatible with a slope of unity; but this comparison is only illustrative.

5. Conclusions

We have presented in this paper the final FIRBACK data reduction using: (1) The Phot Interactive Analysis version 7.2.2 and (2) extra developments (corrections of the flat-field, long and short term transients, transients induced by cosmic rays and adapted reprojection). Most of these extra developments have been made possible by the perfect redundancy inside each raster (one pixel overlap in both Y and Z direction). We have then checked the absolute calibration using PHT25 measurements and the footprint measured on Saturn (compared to the footprint model). We have shown that the ISOPHOT $170\ \mu\text{m}$ extended emission calibration has to be corrected by a factor 0.89, which comes from the difference in solid angle between the PIA v7.2 and the modeled footprint.

³ The difference between Puget et al. 2000 (paper I) FSM1 brightness and the brightness obtained now is less than 6%

⁴ SCANPI is described on the WEB site [http : //www.ipac.caltech.edu/ipac/iras/scanpi_over.html](http://www.ipac.caltech.edu/ipac/iras/scanpi_over.html)

Using this data reduction and calibration, we obtain an absolute calibration which is in remarkable agreement (better than 10%) with brightness extrapolation that uses DIRBE data and HI column density measurements. We have in FIRBACK fields a very high signal to noise ratio (greater than 50). The main limitation comes in fact from the extragalactic source confusion itself (Dole et al. 2001).

Acknowledgements: We would like to thank A. Abergel, C. Gabriel, U. Klaas, M-A. Miville-Deschênes and the ISOPHOT team for many interactions concerning the data reduction and the footprint analysis. We thanks Danny Dale for his help in using the template spectra for IRAS extrapolation. We thank J.L. Puget for his helpful advice all along the data reduction process.

References

- Bethier J., 1998 Notes Scientifiques et Techniques du Bureau des longitudes S060, 1998, <http://www.bdl.fr/ephem/ephepos/>
- Dale D., Helou G. ApJ 2000, in press
- Dole H., Gispert R., Lagache G., et al. 2001, A&A, in press
- Dole H., 2000a, PhD thesis, Paris XI University
- Dole H., 2000b, in ISO Surveys of a Dusty Universe, Lemke, Stickel, Wilke Eds, Springer Lecture Notes, astro-ph/0002283
- Gabriel C., Acosta-Pulido J., Henrichsen I., et al., 1997, ADAAS VI, A.S.P. Conference series, vol. 125, G. Hunt, H.E. Payne eds, p 108
- Hartmann D., Burton W.B., Atlas of Galactic neutral Hydrogen, Cambridge University Press, 1997
- ISO Consortium, The calibration of ISO, ESA technical report, http://www.iso.vilspa.esa.es/users/expl_lib/ISO/wwwcal, 2000a
- ISO Consortium, The ISO handbook v1.0, ESA technical report, http://www.iso.vilspa.esa.es/manuals/-HANDBOOK/V/pht_hb, 2000b
- Kranz T., Lemke D., Toth L.V. et al., ISO/ISOPHOT straylight caused by sun, moon and earth, p 56, 1998
- Klaas U., Lemke D., Kranz T. et al., Infrared straylight measurements of the ISO telescope, p 996, 1998a
- Klaas U., Laureijs R.J., Radovich M., Schulz B., ISOPHOT calibration accuracies, ESA technical report, http://www.iso.vilspa.esa.es/manuals/PHT/-accuracies/pht_accuacies20, 1998b
- Lagache G., 1998, PhD thesis, Paris XI University
- Lagache G., Puget J-L., 2000, A&A 355, 17
- Lagache G., Haffner M.L., Reynolds R.J., Tufte S.L., 2000, A&A 354, 247
- Lemke D., Klaas U., Abraham P. et al., ISOPHOT: inflight performance report, p L627, 1998
- Miville-Deschênes M.A., Abergel A., Boulanger F., Bernard J-P., 2000, A&AS 146, 519
- Oliver S., Rowan-Robinson M., Alexander D.M., et al., 2000, MNRAS 316, 749
- Puget J.L., Lagache G., Clements D.L., et al., 1999, A&A 354, 29
- Puget J.L., Lagache G., Symp. IAU 204, 2001
- Reach W.T., Franz B.A., Kelsall T., et al., 1995, in Unveiling the Cosmic Infrared Background, ed. E. Dwek, AIP Conf. Proc.
- Schulz B., Huth S., Kinkel U. et al., 1999, ESA-SP 426, 965